Climatic Change (2021) 165: 41
https://doi.org/10.1007/s10584-021-03076-2

Relationship of extreme precipitation, surface air temperature, and dew point temperature across the Tibetan Plateau

Zhiwei Yong, et al. *[full author details at the end of the article]*

Received: 17 July 2020 / Accepted: 16 March 2021 / Published online: 31 March 2021

Abstract
Global warming is expected to have profound socio-economic and environmental consequences, and one of the key concerns is extreme precipitation. The classic theory indicates that the variation of extreme precipitation will follow the thermodynamically based Clausius-Clapeyron relation (increasing at a rate of approximately 7%/°C). However, the interaction and the seasonal variation of the relationship between extreme precipitation and temperature has not been thoroughly integrated. Here, we use quantile regression and the binning method to process meteorological station data and the reanalysis data from 78 stations on the Tibetan Plateau (TP), and estimate the sensitivity and dependency of extreme precipitation to both surface air temperature and dew point temperature. The results indicate that the majority of the meteorological stations experience a positive scaling between extreme precipitation and surface air temperature, with the median of surface air temperature scaling close to 2.5%/°C. With regard to scaling during individual seasons, 80% of stations possess negative scaling of the 99th percentile of extreme precipitation with temperature in summer, while 63 stations (81% of the total) display positive trends in winter, and the other 19% have negative scaling. A stronger scaling (3.5%/°C) occurs between dewpoint temperature and extreme precipitation. For surface air temperature < -3 °C and > 8 °C, relative humidity decreases with increasing temperature and dewpoint depression increases, so dewpoint temperature increases more slowly than temperature, resulting in the stronger scaling relationship with dewpoint temperature. The depression of dewpoint temperature presents a slight decrease in −3–8 °C interval, but dewpoint temperature increases faster than other intervals, and the scaling relationship of dewpoint temperature is consistently larger than with surface air temperature due to the small increasing rate with dewpoint temperature and increasing extreme precipitation intensity. Our results emphasize that the increasing temperature has clear scaling and seasonal relationship with extreme precipitation on the TP, and the atmospheric humidity variation has an effect on the overall difference in the scaling relationships of extreme precipitation with surface air temperature and dewpoint temperature. The variations of seasonality and the effects of atmospheric humidity for extreme precipitation should also be carefully considered in future research.

Keywords Extreme precipitation · Surface air temperature · Dew point temperature · Scaling relationship · Seasonal characteristics · Tibetan Plateau

1 Introduction

It is generally accepted that nature and anthropogenic activities will result in climate warming in most regions around the world, which will increase the water vapor holding capacity of the atmosphere, thereby leading to an increase in extreme precipitation (Hoegh-Guldberg et al. 2018; Kharin et al. 2013; Stocker et al. 2013; Zhou et al. 2014). Meanwhile, increasing extreme precipitation events are responsible for more flooding, landslides, and ecological damage, possibly causing loss of life and economic damage (Arshad et al. 2020; Balogun et al. 2020; Knapp et al. 2008; Xiong et al. 2019). Hence, understanding the variations in extreme precipitation in response to global warming is crucial.

Previous research has predicted that the increase in extreme precipitation will follow the physical basis of the Clausius-Clapeyron (C-C) relation (Min et al. 2011; Park and Min 2017). This relation indicates that the capacity of the atmosphere holding moisture should increase with air temperature by about 7%/°C, which is similar to the rate of increasing extreme precipitation (Allen and Ingram 2002; Zhang and Villarini 2017). The C-C relation represents the water vapor holding capacity of the atmosphere and is a benchmark used to interpret variations in extreme precipitation and global mean precipitation (Held and Soden 2006). However, previous studies have indicated that the variation of global mean precipitation (approximately 2–3%/°C) is typically smaller than the C-C rate (Allen and Ingram 2002; Roderick et al. 2014), which reflected that the overall intensity of the water cycle is constrained by the ability of the excess latent heat to be released by precipitation (Zhang et al. 2017). In contrast, variations of extreme precipitation were thought to be predominantly thermodynamic, and thus controlled by the availability of atmospheric moisture (Trenberth 1999). It is postulated that the variations of extreme precipitation from sufficient moisture were consistent with the C-C relation (about 7%/°C); however, extreme precipitation intensity may increase when it is controlled by local moisture convergence (Loriaux et al. 2013). Moreover, observed historical extreme precipitation across global land regions increased at the rate predicted by the C-C relation (Westra et al. 2013). Global climate model (GCM) simulations have produced similar results with those of observations, and the extreme 1-day precipitation was indeed increased at approximately the C-C rate (Kharin et al. 2013; Pall et al. 2007).

Nonetheless, deviations of the C-C relation have been found in many areas of the globe. For instance, sensitivities of extreme precipitation to temperature could be up to 14%/°C (double the C-C rate) in the mid-latitudes (Jones et al. 2010; Lenderink et al. 2011). Moreover, negative rates were often observed in India and other high-temperature regimes (Ali and Mishra 2017). The spatial heterogeneity may be associated with orographic fluctuations, local scale convection, and the dominant precipitation type of a region (Berg et al. 2013). It has also been discovered that the relationship between temperature and extreme precipitation may change with precipitation duration (hourly, daily, and multi-day) (Shaw et al. 2011) and may increase with increasing extreme precipitation percentile (Jones et al. 2010).

Furthermore, the availability of moisture under the influence of global warming is an important issue. Previous researchers have argued that soil moisture deficits and resulting decreases in relative humidity at high temperatures will be the dominant factors limiting the C-C relation (Berg et al. 2009). These limitations in calculating the extreme precipitation scaling may be circumvented by dew point temperature (DPT), which corresponds to the air temperature at which the air is completely saturated with water (Lenderink et al. 2011; Zhang et al. 2019). The scaling of extreme precipitation with DPT possessed greater consistency with the C-C relation (Barbero et al. 2018). The differences between the extreme precipitation scaling

rates using surface air temperature (SAT) and DPT have been explored in a limited number of regions (Ali et al. 2018; Ali and Mishra 2017; Wasko et al. 2018). However, it is still unclear for most areas of the world whether the observed extreme precipitation-temperature sensitivity is more consistent with the C-C relation when the DPT is considered rather than the SAT.

Although some studies have investigated the scaling relationship, spatial heterogeneity, effects of climate dynamics, and surface energy budget of extreme precipitation (O'Gorman and Muller 2010; Panthou et al. 2014; Schroeer and Kirchengast 2017; Willett et al. 2010), the relationship between extreme precipitation and temperature is ambiguous on the Tibetan Plateau (TP). TP is extremely sensitive to global warming, and extreme precipitation exerts an important effect on this region and its surrounding regions (Kang et al. 2010). A report of IPCC had shown that statistically significant changes in heavy precipitation between 1.5 and 2 °C of global warming are located in the TP (Hoegh-Guldberg et al. 2018). It is therefore of interest to explore extreme precipitation on the TP, where the precipitation is controlled by its unique topography and the world's highest average elevation. If understanding whether the variation of extreme precipitation can be explained by SAT and moisture variations based on the C-C relation, then, we will be able to utilize the observed scaling relationship, the seasonal scaling, and the dependency relationship to better predict the influence of global warming on extreme precipitation on the TP (Ali et al. 2018).

In this study, we calculated the scaling relationship of extreme precipitation, SAT, and DPT based on the quantile regression, and applied the binning method to develop the dependency of extreme precipitation to SAT/DPT across the TP during 1980–2015. The goals of our study were to accomplish the following: (1) assessing the relationship of extreme precipitation to SAT/DPT across the TP; (2) evaluating the seasonal scaling of extreme precipitation to SAT/DPT; and (3) analyzing the response of the atmospheric moisture to SAT on the TP.

2 Data sources and methods

2.1 Study area

The Tibetan Plateau, located in southwest China, covers an area of 2.5 million km^2, stretching approximately 2900 km from east (104°47′ E) to west (73°19′ E) and 1500 km from north (39°47′ N) to south (26°00′ N) (Wang et al. 2013). Since the average elevation of the TP is approximately 4500 m, it has been called the *roof of the world* and the *third pole of the Earth* (Ji et al. 2015; Qiu and Jane 2007) (Fig. 1). Moreover, the TP is the source of the major rivers flowing through the surrounding Asian countries, for example, the Yangtze, Yellow, Mekong, Ganges, and Indus Rivers (Chen et al. 2018), providing the main water source for nearly 1.4 billion people. With its distinctive topographic and landscape features, the TP's winter weather is dominated by westerly jet, bringing dry air and high winds. In summer, as a result of the profound effects of the East Asian and South Asian monsoons, temperatures rise and precipitation increases (Duan et al. 2012; Immerzeel and Bierkens 2012). Specifically, the annual mean total precipitation increases from 16 mm in the northwest to 1764 mm in the southeast of the TP, and a corresponding variation gradient in the annual mean air temperature increasing from −5.0 °C in the northwest to 15.5 °C in the southeast from 1981 to 2011 (Chen et al. 2015). Overall, the climate of the TP is characterized by low temperatures, large annual temperature ranges, and sufficient solar radiation, with the spatial pattern exhibiting horizontal band differentiation from warm-humid in the southeast to dry-cold in the northwest (Fig. S1).

2.2 Data sources

Here, we provide a brief description of the observational dataset use in this study. The dataset was obtained from the National Meteorological Information Center (NMIC) of the China Meteorological Administration (CMA) (http://data.cma.cn/), and consists of the daily precipitation, daily mean air temperatures, and relative humidity measurements of 699 meteorological stations. The observational dataset was quality controlled using the NMIC's conventional procedures, including the climatological limit check, extremes check, and consistency checks (Xu et al. 2013). The availability of each data element is generally more than 99%, and the accuracy of the data is close to 100%. Our analysis is restricted to the meteorological stations that had no more than 25% missing data for any of the variables, and in order to apply a dataset which adequately captured the behavior of extremes, meteorological stations with a sufficient record length were required. Imposing a requirement for too long a record, however, limits the available data and the capacity for meaningful analysis (Molnar et al. 2015; Wasko et al. 2018). A length of 36 years was considered an appropriate compromise, with the period 1980–2015 providing the applicable number of 78 meteorological stations on the TP. The locations of the meteorological stations are indicated by dots in Fig. 1.

We also added different reanalysis datasets to compare and verify the results calculated by the observational dataset. We obtained daily climatic data from ERA5 reanalysis dataset on the TP for the period of 1980–2015, with the spatial resolution of 0.25° × 0.25°. The daily ERA5 data were derived from ERA5 hourly data on single levels, and are available from the European Centre for Medium-Range Weather Forecasts website (https://cds.climate.

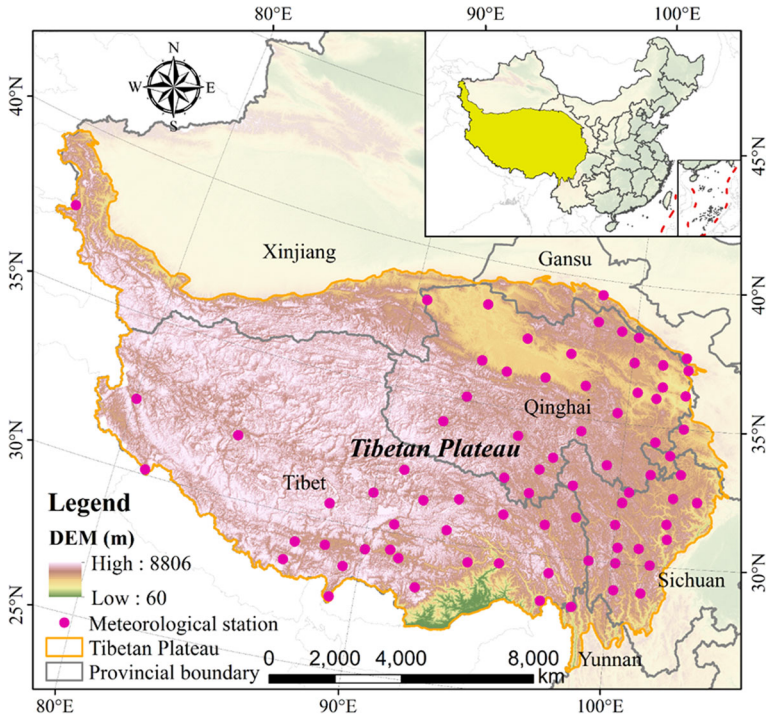

Fig. 1 The study area and locations of meteorological stations, and the geographical position of the Tibetan Plateau in China

copernicus.eu/cdsapp#!/dataset/reanalysis-era5-single-levels?tab=form). Moreover, we also obtained daily climatic data at 0.5° resolution from Climate Forecast System Reanalysis (CFSR) 6-hourly Products dataset and Climate Forecast System Version 2 (CFSv2) Selected Hourly Time-Series Products for the period of 1980–2015, and these datasets is available from the National Centers for Environmental Prediction (NCEP) website (https://rda.ucar.edu/). Among these datasets, CFSR 6-hourly Products dataset was initially completed over the 31-year period from 1979 to 2009 and has been extended to March 2011 (Decker et al. 2010). CFSv2 used the same model that was used to create the NCEP Climate Forecast System Reanalysis (CFSR), and provided the climatic data after December 2010. In order to compare and analyze the results, we extracted the grid data to the nearest meteorological station to calculate the sensitivity and dependency.

We used the basic geographic data compiled from the Resource and Environment Data Cloud Platform (http://www.resdc.cn), which includes the digital elevation model (DEM), the boundary of the TP, provincial boundaries, and national boundaries (Table 1).

2.3 Analytical methods

2.3.1 Calculation of dew point temperature

Relationships between temperature and precipitation are difficult to assess due to the ambiguity of causes and effects (Trenberth and Shea 2005). As discussed in Section 1, on the global and climatic time scale, warmer temperatures are associated with increasing moisture and precipitation. Nevertheless, some studies have revealed that prolonged drought could lead to a soil moisture deficit, with further reductions in surface evaporation and increases in temperature (Vautard et al. 2007).

We circumvent this ambiguity by taking the DPT as a direct measure of moisture in our analyses. The DPT is calculated using daily surface air temperature and the relative humidity (Eqs. 1 and 2) (Zhang et al. 2019):

$$DPT = \frac{257.14 \times Y}{18.678 - Y} \tag{1}$$

where Y can be calculated by the following:

Table 1 Source and resolution of basic geographic data sets

Data	Source
Boundaries data	Flash Flood Investigation and Evaluation Dataset of China, 1949–2015, 1:50,000, vector data.
DEM	Geospatial Data Cloud, 2000, 90 m × 90 m, raster data.
Meteorological observational dataset	the National Meteorological Information Center (NMIC) of the China Meteorological Administration, 1980–2015.
ERA5 reanalysis dataset	the European Centre for Medium-Range Weather Forecasts (ECMWF), 0.25° × 0.25°, 1980–2015, raster data.
CFSR and CFSv2 reanalysis dataset	the National Centers for Environmental Prediction (NCEP), 0.5°×0.5°, 1980–2015, raster data.

$$Y = \log\frac{RH}{100} + \frac{18.678 \times Tas}{275.14 + tas} \tag{2}$$

in which RH represents relative humidity (%), and Tas is the surface air temperature (°C).

The dewpoint depression (DPD) is a way to characterize atmospheric humidity, wherein a small DPD indicates that the atmosphere is close to being saturated, while a large DPD indicates that the atmosphere tends toward being dry (Wang et al. 2019). DPD can be calculated by Eq. 3 as follows:

$$DPD = T - D \tag{3}$$

where T is the SAT, and D is the DPT.

2.3.2 Quantile regression

In most previous studies, the scaling between precipitation and temperature was estimated using the binning method (Blenkinsop et al. 2015; Mishra et al. 2012; Zhang et al. 2017). However, bin size and the outlying data in each bin may affect the scaling estimates (Berg et al. 2009). Therefore, we use quantile regression to evaluate the scaling relationship, which is a more robust and flexible method without additional assumptions (Tan and H.Y 2016; Wasko and Sharma 2014), and it gives a more comprehensive understanding of the effect of temperature on the distribution of extreme precipitation intensity (Schroeer and Kirchengast 2017). The description of quantile regression is as follows (Ali et al. 2018).

We applied quantile regression for a set of pairs (x_i, y_i) of precipitation ($y \geq 0.1$ mm and corresponding temperatures (x). For $i = 1, 2, \ldots, n$, the quantile regression for a given percentile (the 90th, 95th, and 99th percentiles in our study) is calculated by Eq. 4 as

$$\log(y_i) = \beta_0^{(p)} + \beta_1^{(p)} x_i \tag{4}$$

where y_i is the precipitation, x_i is the corresponding temperature (SAT/DPT), and n the is the length of the precipitation-temperature time series. After estimating $\beta_1^{(p)}$ via regression analysis, the scaling of precipitation ($\Delta P\%$) with temperature is derived using an exponential transformation of the regression coefficients (Eq. 5):

$$\Delta P\% = 100 \times \left(e^{\beta_1^{(p)}} - 1\right) \tag{5}$$

We carried out quantile regression analysis using "quantreg" package (available at http://cran.r-project.org/web/packages/quantreg) of R software (R Core Development Team, R Foundation for Statistical Computing, Vienna, Austria) (Koenker 2009).

2.3.3 Binning method

We followed the binning method in order to understand the dependencies of the extreme precipitation percentiles (90th–99.9th) of the observed daily precipitation distribution on temperature (SAT/DPT) (Lenderink and Erik 2010; Lochbihler et al. 2017; Zhang et al. 2017). For each location, we extract wet events (precipitation ≥0.1 mm, defined as a "wet

day") from the period of 1980–2015 and their corresponding daily SAT/DPT based on the observational dataset and reanalysis datasets. Precipitation on the wet days was placed in moving 2 °C temperature bins (ordered from lowest to highest), with roughly the same number of wet days in each, and a 1 °C overlap between bins. This is done to avoid a dependence of the plot appearance on the arbitrary choice of the binning intervals, which sometimes occurs when the amount of observation data is limited (Lenderink et al. 2011). In addition, previous study found that extreme precipitation intensity changes more smoothly with an interval of 2 °C (Wang et al. 2019). Within each 2 °C bin, the different extreme percentiles (90th, 95th, 99th, and 99.9th percentiles) of wet-day precipitation amounts as well as the median of temperature were estimated. Similarly, we scaled different extreme percentile precipitation with DPT.

2.4 Psychrometric chart

Figure 2 is a psychrometric chart pertaining to conditions on the TP. This chart illustrates changes for a temperature starting at 10 °C and 60% relative humidity (point T_1 with dewpoint temperature DPT_1 and DPD 7.5 K). If the parcel warms 10 K with fixed relative humidity (arriving at point T_{2b}), the DPD stays almost the same (changing to 8 K) and DPT warms almost the same amount (9.5 K) as SAT. If relative humidity decreases from 60 to 50% (arriving at point T_{2a}), the DPD increases and DPT increases more slowly than SAT (an increase from DPT_1 to DPT_{2a} is only 6.5 K). Conversely, when relative humidity increases, the DPD decreases and DPT increases faster than SAT (as seen with warming to points T_{2c} and T_{2d}). It can also be seen that the change in DPD plus the change in DPT equals the change in SAT plus the original DPD for all cases.

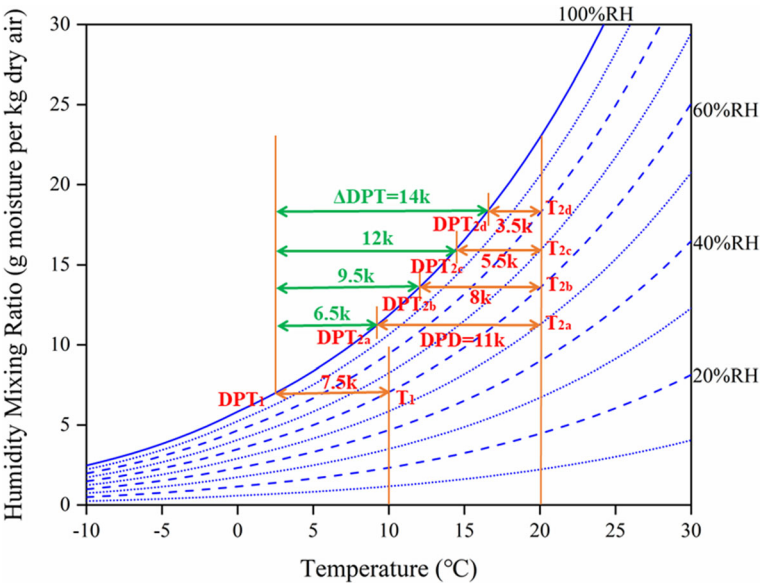

Fig. 2 Psychrometric chart on the Tibetan Plateau

3 Results

3.1 Scaling of daily extreme precipitation

The scaling results of both SAT and DPT are calculated using quantile regression for 78 stations across the TP (Fig. 3). Inspecting Fig. 3 a, at least two broadly distinct regions can be seen: the southwest region of the TP where the scaling of the 90th percentile of extreme precipitation with SAT is negative, especially in the Lazi station (−7.13%/°C), and the 19 stations generally that exhibit a positive trend at a rate exceeding 3.5%/°C. For the 95th percentile (Fig. 3b) and 99th percentile (Fig. 3c), the results were broadly similar, while the number of stations with the scaling >3.5%/°C decreases at the higher threshold. The scaling of the extreme precipitation threshold to DPT is slightly different. For the 90th percentile (Fig. 3d), the majority of the meteorological stations (55%) on the TP exhibited positive precipitation scaling with many observatories between the 0.5 C-C relation (3.5%/°C) and the C-C relation (7%/°C). For the spatial patterns of the 95th/99th percentiles, more consistent results are found. The majority of the TP shows approximately 2–5%/°C scaling.

The shift in the distribution of the scaling is presented in Fig. 3a–c. For the 90th percentile (Fig. 4a), the asymmetrical distribution shifted the center to approximately 2.73%/°C when SAT was used above the 0.5 C-C relation (albeit with a small range) for DPT. For the 95th percentile (Fig. 4b), a similar asymmetrical distribution centered just below the 0.5 C-C relation was observed for DPT, whereas the median SAT scaling was close to 2.5%/°C. Inspecting Fig. 4c, the entire distribution centered of the 99th percentile could be identified

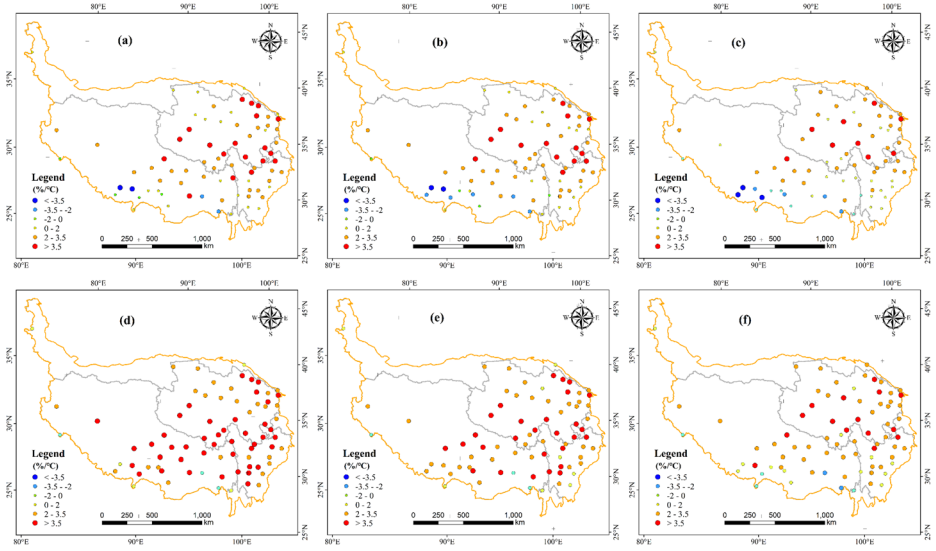

Fig. 3 Scaling relation between extreme precipitation and SAT/DPT for 78 stations on the Tibetan Plateau with periods of 1980–2015. **a** 90th percentile extreme precipitation and SAT; **b** 95th percentile extreme precipitation and SAT; **c** 99th percentile extreme precipitation and SAT; **d** 90th percentile extreme precipitation and DPT; **e** 95th percentile extreme precipitation and DPT; **f** 99th percentile extreme precipitation and DPT. The color and size of the legend markers indicate the scaling slope magnitude in %/°C

near 2.5%/°C. Figure 4d illustrates the dependence of the daily extreme precipitation derived using the binning method from the 78 stations on the TP. For TP, there was a clear hint of stability in extreme precipitation intensity for temperatures above 0 °C, with the DPT exhibiting a similar pattern. Below 0 °C, the 90th, 95th, and 99th percentile extreme precipitation exhibits similar approximately 0.5 C-C scaling, while the scaling of the 99.9th percentile extreme precipitation threshold is close to the C-C scaling. These results using the DPT are plotted in Fig. 4 e. All extreme precipitation percentile thresholds displayed temperature dependencies similar to those of the SAT observations.

Furthermore, we evaluate the robustness of our observational results by comparing the scaling relationship obtained from the observational dataset and the two reanalysis datasets (ERA5 and CFSR). Based on the quantile regression and binning method, we find a consistent scaling relationship between extreme precipitation and SAT/DPT from the observational dataset and two reanalysis datasets (Fig. S2, S4). Finally, the median SAT scaling is distributed between 2 and 4%/°C, and the dependencies of different extreme percentiles (90th–99.9th) show similar trends (Fig. S3, S5).

3.2 Seasonal scaling of daily extreme precipitation

We begin our analysis to estimate the seasonal scaling of the daily extreme precipitation by using SAT and DPT (Figs. 5 and 6). In spring (March to May), we find that the distribution of scaling is somewhat similar between SAT and DPT. For instance, the positive scaling tendency for most of the meteorological stations is consistent for 90th, 95th, and 99th percentiles. However, all observatories located on the TP have scaling rate at less than 7%/°C in spring (Fig. 5 a–c, Fig. 6a–c). For the summer (June to August), the distinct negative

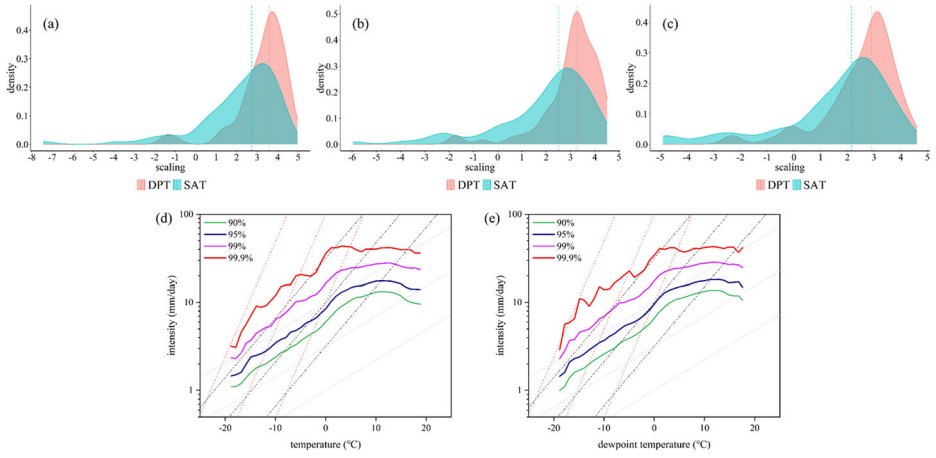

Fig. 4 Density of **a** 90th, **b** 95th, and **c** 99th percentile extreme precipitation scaling (%/°C) across the Tibetan Plateau. Green indicates SAT scaling, orange represents DPT scaling, and the dotted line represents the median of the scaling; **d** Dependencies of different extreme percentiles (90th–99.9th) of the observed daily precipitation distribution on SAT; **e** Dependencies of different extreme percentiles (90th–99.9th) of the observed daily precipitation distribution on DPT. Solid lines are percentiles computed from the raw data, while dotted lines are the exponential relationships given by 0.5 (light gray), 1 (black), and 2 (dark red) times the C-C relation. Note the logarithmic *y*-axis

scaling of extreme precipitation can be seen in the south of the TP, and the negative scaling of SAT is shown at 87%, 82%, and 79% observatories for the 90th, 95th, and 99th percentiles, respectively (Fig. 5d–f). Moreover, the scaling of DPT at most of the observatories also shows negative trends, and which are distributed in the southern plateau (Fig. 6d–f). In autumn (September to November), the scaling for most of the

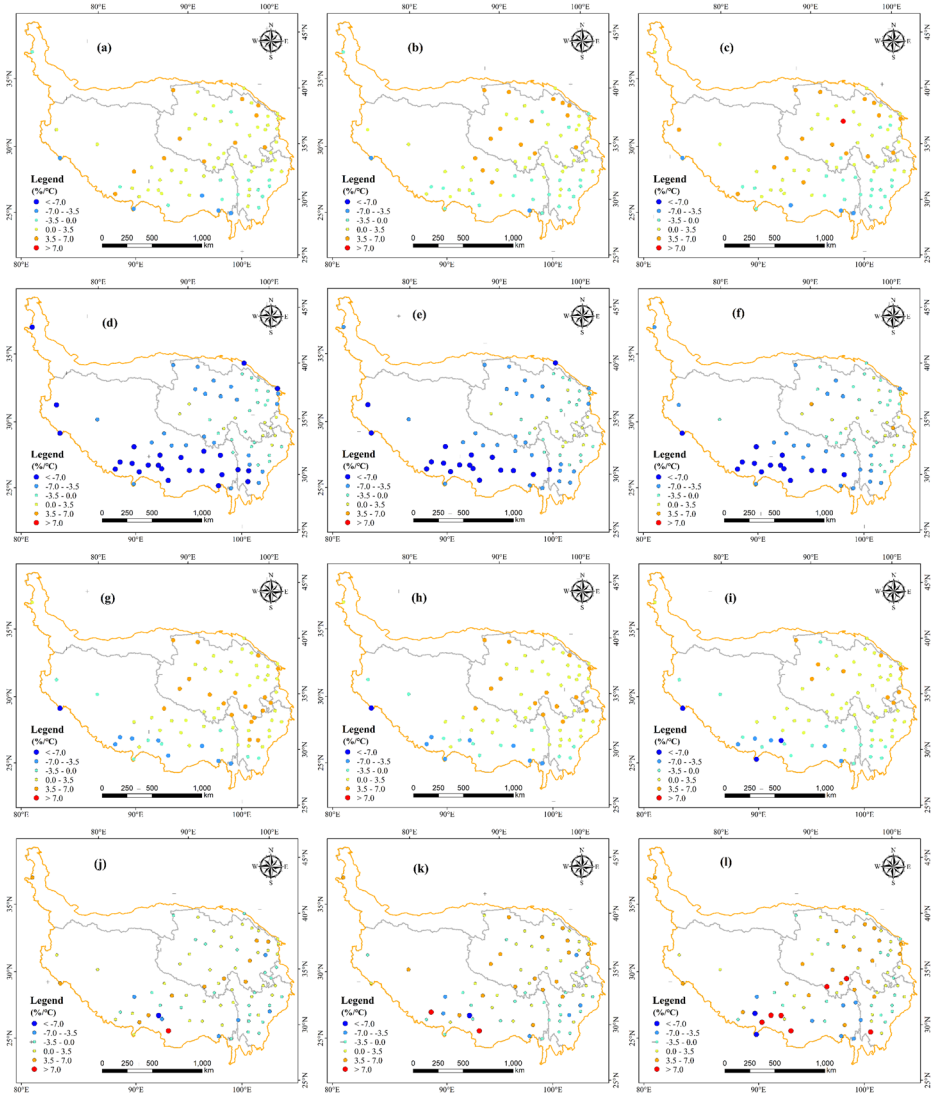

Fig. 5 Spatial maps of seasonal scaling slopes of extreme precipitation intensity for SAT. **a**–**c** 90th, 95th, and 99th percentile extreme precipitation and SAT in spring (MAM); d–f 90th, 95th, and 99th percentile extreme precipitation and SAT in summer (JJA); **g**–**i** 90th, 95th, and 99th percentile extreme precipitation and SAT in autumn (SON); **j**–**l** 90th, 95th, and 99th percentile extreme precipitation and SAT in winter (DJF). The color and size of the legend markers indicate the scaling slope magnitude in %/°C

observatories is similar to spring (Fig. 5g–i, Fig. 6g–i). For winter (December to February), the 99th percentile extreme precipitation of winter displays a positive scaling with SAT at 67.7% of stations and super C-C scaling (> 7%/°C) at 7 locations (Fig. 5l). Nevertheless, the winter scaling between the 99th percentile extreme precipitation and DPT is positive at most of locations (80.8%), and super C-C scaling is found at 14 stations (Fig. 6l). The scalings of the 90th and 95th percentile extreme precipitation with

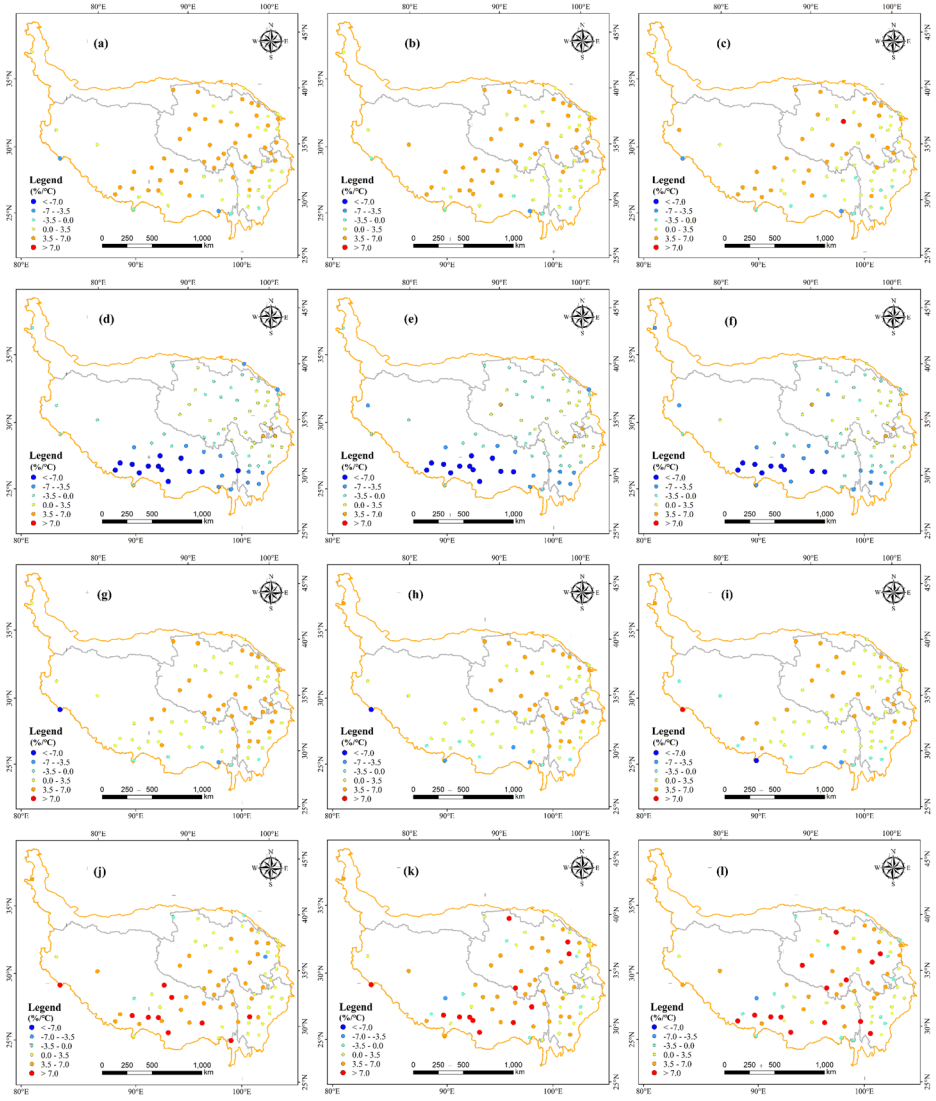

Fig. 6 Spatial maps of seasonal scaling slopes of extreme precipitation intensity for DPT. a–c 90th, 95th, and 99th percentile extreme precipitation and DPT in spring (MAM); **d–f** 90th, 95th, and 99th percentile extreme precipitation and DPT in summer (JJA); **g–i** 90th, 95th, and 99th percentile extreme precipitation and DPT in autumn (SON); **j–l** 90th, 95th, and 99th percentile extreme precipitation and DPT in winter (DJF). The color and size of the legend markers indicate the scaling slope magnitude in %/°C

SAT/DPT are generally consistent with those of the 99th percentile precipitation (Fig. 5 j–k Fig. 6j–i).

Figure 7 summarizes the results of this analysis. Including all 90th percentile extreme precipitation events for the SAT/DPT, the scaling varies between −7.4 and 5.0%/°C. From the scaling analysis, we obtain smaller scaling rates, and most of which are less than 0 in summer (Fig. 7a). For winter, the median scaling of the 90th percentile extreme precipitation for the SAT was 0.8%/°C, which is less than the 0.5 C-C rate, while the DPT slope is 3.7%/°C, which is close to the 0.5 C-C rate (Fig. 7a). In spring and autumn, the median scaling for SAT is below the 0.5 C-C relation, but the median scaling for DPT is close to, even exceed 3.5%/°C (Fig. 7a). Similarly, for 95th percentile (Fig. 7b) and 99th percentile (Fig. 7c) extreme precipitation, the scaling of all events exhibits small rates. In summer, the median of the scaling is <0. We find that the median scaling of the SAT is less than the 0.5 C-C relation, while the median scaling of the DPT is greater than the 0.5 C-C relation in winter. Results for the summer period (JJA) are characterized by stable scaling over the entire SAT range from 1 and 19 °C (Fig. 8b). The winter period (DJF) shows a dependence of the daily extreme precipitation on SAT, mostly along the 0.5 C-C line with the exception of temperatures > −5 °C (Fig. 8d). Similar results are obtained when using DPT instead of SAT (Fig. 8h). For spring, the dependence tendencies are consistent for annual values and the spring, a stable dependence is be found for temperatures above 0 °C, and the dependencies of extreme precipitation on SAT/DPT mostly follow 0.5 C-C line (Fig. 8a, e). Furthermore, the overall dependence during autumn is similar to the spring season; however, the dependencies of extreme precipitation follow approximately a C-C line for temperatures below 0 °C (Fig. 8c, g).

In addition, the seasonal scaling obtained with ERA5 and CFSR reanalysis datasets contrasts with the seasonal scaling obtained using the observational dataset. For the spring, autumn, and winter seasons, some similar scaling relationships from the observational dataset, ERA5, and CFSR datasets are displayed. However, we also notice that the scaling shows different variations between the observational dataset and two reanalysis datasets in summer (Fig. S6-S9). Specifically, our results show that these dependencies results obtained using binning method for the observational dataset and reanalysis datasets are consistent (Fig. S10-S13).

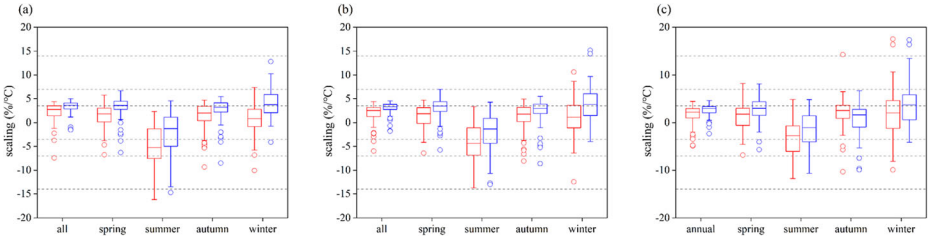

Fig. 7 Box plots showing the distributions of scaling for extreme precipitation intensity at the **a** 90th percentile, **b** 95th percentile, and **c** 99th percentile on an annual and seasonal basis. The red box represents SAT, and the blue box represents DPT. The red and blue lines within the boxes denote the median; the upper and lower bounds are the 25th and 75th percentiles (25P and 75P), respectively. The whiskers are calculated as 75P ± 1.5 (75P–25P). Outliers are plotted as red and blue circles. The horizontal gray dashed lines depict the 0.5 C-C rate (3.5%/°C), C-C rate (7%/°C), and twice C-C rate (14%/°C)

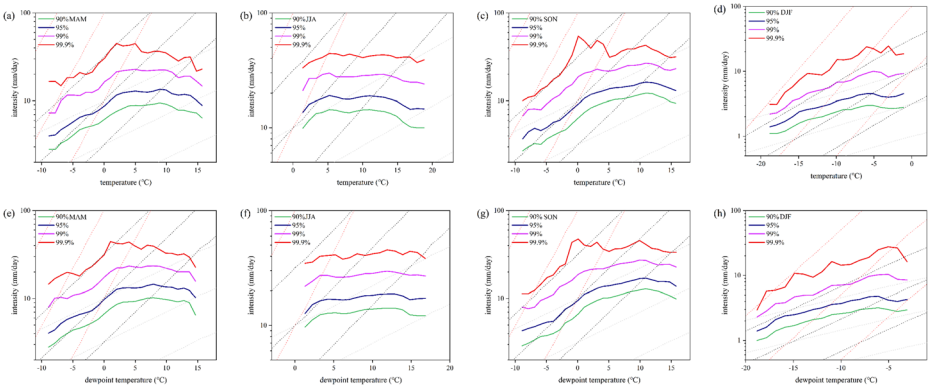

Fig. 8 Seasonal dependencies of extreme percentile intensities (90th–99.9th) of the observed daily precipitation distribution in **a** spring (MAM), **b** summer (JJA), **c** autumn (SON), and **d** winter (DJF); variation of extreme precipitation intensity and DPT in **e** spring (MAM), **f** summer (JJA), **g** in autumn (SON), and **h** winter (DJF). Solid lines are percentiles computed from the raw data. Dotted lines are the exponential relationships given by 0.5 (light gray), 1 (black), and 2 (dark red) times the C-C relation, respectively. Note the logarithmic *y*-axis

3.3 Relationship between atmospheric humidity and SAT

The relationship between the depression of the DPT (DPD) and SAT is presented in Fig. 9. The variation of DPD with SAT for all wet days is shown in Fig. 9 a, revealing that the DPD increases more significantly below −3 °C and above 8 °C on the TP. We estimate that the scaling relationship differs for temperatures inside and outside the −3–8 °C interval (Table 2), with the largest scaling of the 90th percentile of extreme precipitation in the −3 to 8 °C and the largest scaling of the 99th percentile in the < −3 °C interval, but for any interval or percentile, the scaling with DPT is stronger than with SAT. For temperatures above 8 °C, the scaling with SAT is negative while the scaling with DPT is positive. With regard to scaling during individual seasons, Fig. 9 c indicates that the DPD generally increases with increasing temperature, and increases significantly at temperature > 10 °C in summer. Similar increasing trends also occur in winter with subtle differences based on the binning method (Fig. 9e). For the spring season, the DPD shows a stable variation below 5 °C, and a slightly increasing trend is illustrated above 5 °C (Fig. 9b). In autumn, we find that the DPD displays a slightly decreasing trend below 5 °C, and the trends of SAT above 5 °C are similar to those of the spring season (Fig. 9d).

Figure 10 illustrates the spatial patterns of the scaling slopes of the DPD for SAT on the TP from 1980 to 2015. The scaling rates of the 78 stations for the 90th percentile DPD with SAT were calculated, and the results demonstrate that the non-significant slopes mainly occur in most of observational stations. For instance, the scaling slopes of about 92% stations are distributed between −2 and 2%/°C, and only three stations exceed the half C-C relation (3.5%/°C) (Fig. 10a). Moreover, these results of the 95th percentile and the 99th percentile DPD are consistent with the 90th percentile, albeit with some differences for the higher thresholds. In particular, the number of stations where the scaling exceeds the half C-C relation declines for the 95th and 99th percentile DPD (Fig. 10b, c).

Additionally, we find a good agreement between the dependency relationships obtained from two reanalysis datasets and with those obtained from the observational data (Fig. S14,

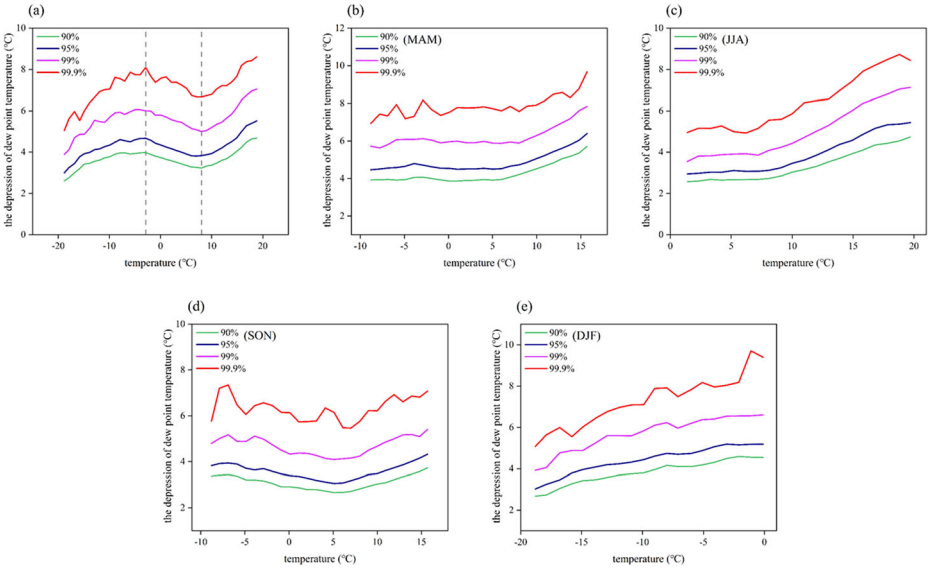

Fig. 9 The relationship between the daily depression of the DPT (DPD) and the SAT in the Tibetan Plateau during 1980–2015. **a** All wet days, **b** wet days in spring (MAM), **c** wet days in summer (JJA), **d** wet days in autumn (SON), and **e** wet days in winter (DJF). The green, blue, purple, and red lines denote the variation of the 90th, 95th, 99th, and 99.9th percentiles of DPD with SAT, respectively, while the gray dotted lines indicate the temperature transition values

S16), and the scaling results of different percentile extreme precipitation also are primarily distributed between −2 and 2%/°C (Fig. S15, S17).

4 Discussion

4.1 Relationship of SAT with extreme precipitation

On a climatic time scale, warmer temperature is associated with increasing moisture, and thus leads to increased precipitation (Lenderink et al. 2011; Stocker et al. 2013). Our study shows that the majority of the meteorological stations on the TP exhibit positive scaling of extreme precipitation with SAT (Fig. 2a–f), and a consistent scaling relationship from the ERA5 and CFSR reanalysis dataset is found on the TP (Fig. S1, S3). This result indicates that the positive scaling relationship of extreme precipitation on the TP is similar to that on a global scale. The TP is considered to be a climate precursor area, which is more sensitive to global climate

Table 2 The scaling relationship of extreme precipitation in different temperature intervals

Temperature	Precipitation	<−3 °C	−3–8 °C	>8 °C
SAT	90th percentile	3.92%/°C	4.19%/°C	−1.24%/°C
	95th percentile	4.02%/°C	3.85%/°C	−0.88%/°C
	99th percentile	4.37%/°C	2.84%/°C	−0.54%/°C
DPT	90th percentile	4.88%/°C	6.34%/°C	1.44%/°C
	95th percentile	4.80%/°C	5.78%/°C	1.31%/°C
	99th percentile	5.16%/°C	4.65%/°C	1.15%/°C

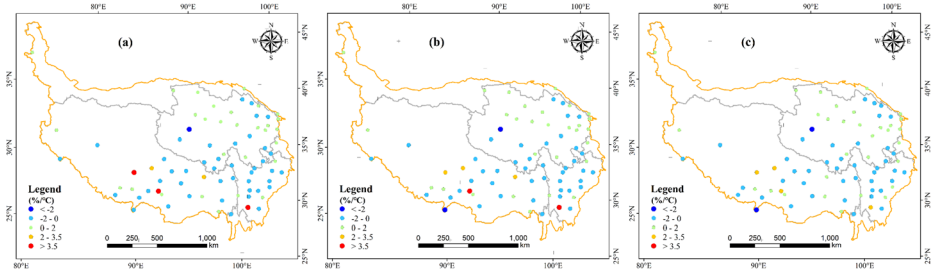

Fig. 10 Spatial maps of scaling slopes of **a** 90th, **b** 95th, and **c** 99th percentile daily depression of the DPT (DPD) for SAT on the Tibetan Plateau during 1980–2015. The color and size of the legend markers indicate the scaling slope magnitude in %/°C

warming (Kang et al. 2010). However, we also find that Lazi and its surrounding stations present a negative scaling relationship. Other research has found that the negative scaling is dominated by less precipitation, which favors more sunshine and less evaporative cooling (Trenberth and Shea 2005). Therefore, the negative scaling rate in Lazi station and its surrounding stations have been attributed to more sunlight, resulting in less soil moisture and a higher SAT in those regions (Chen et al. 2007).

On the TP, the dependencies of the observed daily precipitation on SAT expressed a similar distribution for each percentile and clearly display a stable trend above 0 °C and approximately 0.5 C-C scaling below 0 °C (Fig. 3a–e). At present, the classical argument is that the scaling between extreme precipitation and temperature should be consistent with the C-C relation (Zhao et al. 2012). However, there is no reason why extremes should follow the C-C relation exactly. For example, changes in the atmospheric dynamics, convective clouds, and moist adiabatic temperature profiles all could cause deviations from the C-C scaling (O'Gorman and Schneider 2009; Trenberth et al. 2003). In general, precipitation on the TP is mainly in the form of deep convection (Fu et al. 2018). The scaling between deep convective precipitation and temperature is stable when the temperature is above 0 °C (Wang et al. 2019). Compared with stratified precipitation, the sensitivity of deep convective precipitation to temperature is less obvious. The second reason is most likely due to moisture on the TP not being locally sourced, leading to weaker temperature sensitivities (Schroeer and Kirchengast 2017; Zhang et al. 2017). Furthermore, for temperatures lower than 0 °C, precipitation events are considered to be snow events. Increased snow depth has occurred on the TP since the mid-1970s (Zhu et al. 2015), the result of an intensified subtropical westerly jet and enhanced ascending motion over the region; hence, this research provides direct evidence for primarily positive trend exhibited by the winter scaling (Fig. 4j–l). Local moisture is reduced, while anomalous ascending moisture advection leads to more precipitation over the TP (Bao and You 2019). In contrast, for the summer negative scaling in the low latitudes of the TP, the SAT is often cooled due to precipitation, resulting in the negative sensitivity between summer SAT and precipitation (Ali and Mishra 2017). In spring and autumn, the scaling relationship is transitional between that of winter and summer, with a general increase at low temperatures and a stable trend at higher temperatures (Fig. 7a, d). The observational dataset and two reanalysis datasets show a high degree of agreement in the periods of 1980–2015. Moreover, previous study has also demonstrated that radiative forcing by greenhouse gases is currently suppressing global precipitation at the rate of −0.15%/decade (Allan et al. 2013). Specifically, other factors have been thought to influence the scaling behaviors of extreme precipitation at higher temperatures, for example, the influence of convective fields or systems (Berg et al. 2013),

the presence of lightning (Molnar et al. 2015), El Niño events (Allen and Luptowitz 2017), orography (Drobinski et al. 2016), and anthropogenic aerosols (Gang et al. 2011).

4.2 Relationship of DPT with extreme precipitation

The relationship between DPT and extreme precipitation clearly reflects the effect of moisture on precipitation, and we find that the dependence of extreme precipitation on the DPT even exhibits a median scaling of approximately 3.5%/°C (Fig. 3d–f), which exceeds the 2.5%/°C SAT median scaling. This result is consistent with previous studies, indicating that the improved representation of extreme precipitation variations is possible with DPT, a metric that specifically accounts for the variations in relative humidity, which better reflects the responses of moisture in the atmosphere to surface warming (Zhang et al. 2019). In addition, our results show that relative humidity decreases with increasing temperature and dewpoint depression increases when SAT is below −3 °C and above 8 °C (Fig. 9a). Based on the psychrometric chart (Fig. 2), DPT increases more slowly than SAT, resulting in the stronger scaling relationship with DPT. It is worth noting that DPD shows a slight decrease in the −3–8 °C interval rather than increasing (Fig. 9a), which causes a faster increase in DPT than otherwise (Fig. 2), and faster than in other intervals. However, the scaling relationship with DPT is consistently larger than with SAT. Based on quantile regression, both precipitation intensity and DPT show an increasing trend in the −3–8 °C interval (Fig. S19), so the regression coefficients may not be weaker, and the scaling relationship with DPT will not decrease. In addition, Table 2 shows a small negative scaling relationship with SAT, and a small positive scaling relationship with DPT above 8 °C. Here, as a result of evaporative cooling from precipitation, high SAT becomes cooler during the precipitation day. SAT cooling means that extreme precipitation on the TP occurs on lower temperature days, and the warmer days have fewer and less intense precipitation events, resulting in a negative apparent scaling (Ali et al. 2018; Bao et al. 2017). Moreover, relative humidity increases during the precipitation day, DPT increases when DPD decreases, which indicates extreme precipitation occurs on high DPT days, resulting in a positive scaling. Therefore, changes in DPT may well be more robust and more predictable than variations in SAT (Lenderink et al. 2011). Furthermore, we discovered that the scaling of DPT exhibits a variation similar to that of SAT on the TP (Fig. 4d–e). On wet days, the variations in SAT and DPT are closely linked (Wasko and Nathan 2019). This is consistent with other research results indicating that on regional and global scales, changes in temperature are similar regardless of the type of temperature metric used (Lenderink and Attema 2015).

In summer, our study demonstrates that the median scaling between extreme precipitation and DPT is <0%/°C (Fig. 7a–c). This result is attributed to the decreasing relative humidity with increasing temperature on the TP. The dependency relationship between DPD and SAT shows a consistent result in summer season, and the increasing DPD revealed that local atmospheric humidity decreases with increasing SAT (Fig. 9c). When atmospheric humidity does not increase, the air mass can only rise when it reaches saturation. Therefore, the maximum water vapor content in the lower levels is larger than the maximum at upper levels (Barbero et al. 2018; Drobinski et al. 2016). In addition, water vapor condenses into raindrops, causing the loss of atmospheric water vapor by precipitation. Against the backdrop of global warming, the loss of atmospheric humidity exerts an effect on the precipitation efficiency, further weakening the precipitation intensity (Fig. S18). Furthermore, we noticed that the scaling showed different variations between the observational dataset and two reanalysis

datasets in summer, and previous research also found that extreme precipitation scaling in reanalysis data was different with the observational dataset in the most of mid-latitudes (Zhang et al. 2019). In winter, the trends of extreme precipitation could be explained reasonably well by moisture changes, again with a dependence close to 3.5%/°C (Fig. 7), which is attributed to the anomalous ascending moisture advection leading to more precipitation and snowfall over the TP (Forsythe et al. 2017).

4.3 Relationship of atmospheric humidity with SAT

According to the Clausius-Clapeyron equation, atmospheric humidity is the link between extreme precipitation and SAT. To further investigate how atmospheric humidity affects the relationship between precipitation intensity and SAT on the TP, the relationship between DPD and SAT was explored. Our study indicated that the DPD increased more significantly at temperatures < −3 °C and > 8 °C in TP, while exhibiting a decreasing trend between −3 and 8 °C (Fig. 9a). When the temperature is lower, the actual vapor pressure is strictly controlled by the C-C curve, and the relative humidity increases. For higher temperatures, however, the actual vapor pressure slightly decreases or remains stable and the relative humidity sharply decreases, tending the atmosphere toward being dry, and sharply decreasing extreme precipitation. In this situation, extreme precipitation decreases due to high temperatures and insufficient moisture capacity (Hong et al. 2018). In addition, the spatial patterns of the DPD scaling slopes revealed that the unapparent variation (between −2 and 2%/°C) mainly occurred in the most of observational stations, which indicated that the humidity on the TP was not sensitive to SAT. The possible reasons are that moisture on the TP was not locally sourced, the winter moisture is dominated by westerly jet, and as a result of the profound effects of the East Asian and South Asian monsoons in summer (Duan et al. 2012). Note that the scaling rates using two reanalysis datasets are in good agreement with the observational dataset.

4.4 Importance and uncertainties

Extreme precipitation shows an increasing trend with the global warming. Our study used quantile regression and binning method to analyze meteorology observational data and the reanalysis data from 78 stations on the TP, and estimated the scaling relationship and dependency of extreme precipitation to both SAT and DPT across the TP. Because bin size and the outlying data in each bin may affect the scaling estimates in binning method (Ali and Mishra 2017), we used quantile regression to evaluate the scaling relationship and seasonal scaling characteristics of extreme precipitation during 1980–2015, and which could provide more robust and flexible scaling relation (Wasko and Sharma 2014). The scaling relation shows the sensitivity of extreme precipitation to temperature and its different seasonal characteristics. Moreover, we used the binning method to understand the dependencies of the extreme precipitation percentiles with SAT and DPT, which indicate the variation of extreme precipitation in different temperature intervals (Zhang and Villarini 2017). Then, we have calculated the depression of the DPT to evaluate the relation of atmospheric humidity with SAT (Wang et al. 2019). Finally, we added different reanalysis datasets to compare the consistency with the results of observational dataset, to give more robust conclusions (Zhang et al. 2019). Our study highlights the scaling relationships between extreme precipitation and SAT/DPT, their seasonal characteristics, and the variation of extreme precipitation in different temperature intervals on the TP, which is salutary for future studies regarding the effect of climate change on extreme precipitation.

Despite progress being made via this study, large uncertainties remain. The link of extreme precipitation to temperature used in this study was conservative since it includes only included a few factors out of the many that affect climate. The findings of this study should be considered in light of the following limitations. In this research, the scaling of extreme precipitation with SAT/DPT adopted the daily precipitation rather than short-duration precipitation. The daily precipitation used in this study may produce deviations in the assessment results of short-duration precipitation (Shaw et al. 2011). Moreover, the relationship between extreme precipitation and temperature is complex and challenging. For example, orography (Drobinski et al. 2016), atmospheric dynamics (Berg et al. 2013), and anthropogenic aerosols (Gang et al. 2011) are three additional key factors in extreme precipitation. Therefore, future works will need to focus on atmospheric stability, the effects of aerosols, and other elements that affect the variation in extreme precipitation with temperature across the TP.

5 Conclusions

Our study focuses on the responses of extreme precipitation to temperature increase. Specifically, we analyze the scaling relation between extreme precipitation and SAT/DPT across the TP based on station observation data and reanalysis datasets, and evaluated the link of atmospheric humidity to SAT. In conclusion, the majority of the TP meteorological stations exhibit a positive scaling relationship of extreme precipitation with SAT, which indicates that the variation of extreme precipitation on the TP has a similar trend to that at the global scale. In addition, the scaling variation shows some clear seasonal characteristics, which tend toward a negative trend in summer, but a positive trend in winter. The dependencies of extreme precipitation on SAT displays a stable trend above 0 °C and approximately 0.5 C-C scaling below 0 °C. These results are attributed to the influence of the deep convective precipitation and westerly jet on the winter season of the TP. Next, the DPT results were analyzed; we found that the scaling variations are similar to those of SAT, while the scaling rate of extreme precipitation with DPT is larger than with SAT. Therefore, DPT can better reflect the sensitivity of extreme precipitation to global warming on the TP. Finally, DPD displays an increasing trend when the temperatures are either < -3 °C or > 8 °C, which indicates that DPT increases more slowly than SAT, resulting in the stronger scaling relationship with DPT. However, DPD decreases slightly between −3 and 8 °C, but the scaling relationship of DPT is consistently larger than with SAT. This study provides information regarding the scaling relationship and the seasonal characteristics of extreme precipitation with SAT and DPT, and the dependency of extreme precipitation and atmospheric humidity in different temperature conditions. In the future, incorporating the variations of humidity and the effects of seasonality on extreme precipitation is helpful for producing robust relationship on the TP.

Supplementary Information The online version contains supplementary material available at https://doi.org/10.1007/s10584-021-03076-2.

Author contribution Z.Y. and J.X. designed research; J.X. and Z.W. collected the data; Z.Y. and Q.P. analyzed data; Z.Y. wrote the paper; Z.Y., J.Y. and W.C. provided critical revisions to the paper.

Funding This research was funded by Strategic Priority Research Program of the Chinese Academy of Sciences (Grant No. XDA20030302), the Science and Technology Project of Xizang Autonomous Region (Grant No. XZ201901-GA-07), the National Flash Flood Investigation and Evaluation Project (Grant No. SHZH-IWHR-

57), the Southwest Petroleum University of Science and Technology Innovation Team Projects (Grant No. 2017CXTD09), and the Key R & D project of Sichuan Science and Technology Department (Grant No. 2021YFQ0042).

Declarations

Conflict of interest The authors declare no competing interest.

References

Ali H, Mishra V (2017) Contrasting response of rainfall extremes to increase in surface air and dewpoint temperatures at urban locations in India. Sci Rep 7:1228

Ali H, Fowler HJ, Mishra V (2018) Global observational evidence of strong linkage between dew point temperature and precipitation extremes. Geophys Res Lett 45:12320–12330. https://doi.org/10.1029/2018gl080557

Allan RP, Liu C, Zahn M, Lavers DA, Koukouvagias E, Bodas-Salcedo A (2013) Physically consistent responses of the global atmospheric hydrological cycle in models and observations. Surv Geophys 35: 533–552

Allen MR, Ingram WJ (2002) Constraints on future changes in climate and the hydrologic cycle. Nature 419: 224–232

Allen RJ, Luptowitz R (2017) El Niño-like teleconnection increases California precipitation in response to warming. Nat Commun 8:16055

Arshad A, Ashraf M, Sundari RS, Qamar H, Wajid M, M-u H (2020) Vulnerability assessment of urban expansion and modelling green spaces to build heat waves risk resiliency in Karachi. International Journal of Disaster Risk Reduction 46:101468. https://doi.org/10.1016/j.ijdrr.2019.101468

Balogun A-L et al (2020) Assessing the potentials of digitalization as a tool for climate change adaptation and sustainable development in urban centres. Sustain Cities Soc 53:101888. https://doi.org/10.1016/j.scs.2019.101888

Bao Y, You Q (2019) How do westerly jet streams regulate the winter snow depth over the Tibetan plateau? Clim Dyn 53:353–370

Bao J, Sherwood SC, Alexander LV, Evans JP (2017) Future increases in extreme precipitation exceed observed scaling rates. Nat Clim Chang 7:128–132

Barbero R, Westra S, Lenderink G, Fowlera HJ (2018) Temperature-extreme precipitation scaling: a two-way causality? Int J Climatol 38:e1274–e1279. https://doi.org/10.1007/s10712-012-9213-z

Berg P, Haerter JO, Thejll P, Piani C, Hagemann S, Christensen JH (2009) Seasonal characteristics of the relationship between daily precipitation intensity and surface temperature. J Geophys Res Atmos 114: D18102

Berg P, Moseley C, Haerter JO (2013) Strong increase in convective precipitation in response to higher temperatures. Nat Geosci 6:181–185

Blenkinsop S, Chan SC, Kendon EJ, Roberts NM, Fowler HJ (2015) Temperature influences on intense UK hourly precipitation and dependency on large-scale circulation. Environ Res Lett 10:054021. https://doi.org/10.1088/1748-9326/10/5/054021

Chen X, Zhou J, Zhou H (2007) Assessing danger degree of soil erosion in Rikaze prefecture, Tibet. Wuhan University Journal of Natural Sciences 12:705–709

Chen X, An S, Inouye DW, Schwartz MD (2015) Temperature and snowfall trigger alpine vegetation green-up on the world's roof. Glob Chang Biol 21:3635–3646

Chen X, Long D, Hong Y, Hao X, Hou A (2018) Climatology of snow phenology over the Tibetan plateau for the period 2001-2014 using multisource data. Int J Climatol 38:2718–2729. https://doi.org/10.1002/joc.5455

Decker M, Brunke MA, Wang Z, Sakaguchi K, Zeng X, Bosilovich MG (2010) Evaluation of the reanalysis products from GSFC, NCEP, and ECMWF using flux tower observations. J Clim 25:1916–1944

Drobinski P, Alonzo B, Bastin S, Silva ND, Muller C (2016) Scaling of precipitation extremes with temperature in the French Mediterranean region: what explains the hook shape? J Geophys Res Atmos 121:3100–3119

Duan A, Wu G, Liu Y, Ma Y, Zhao P (2012) Weather and climate effects of the Tibetan Plateau. Adv Atmos Sci 29:978–992. https://doi.org/10.1007/s00376-012-1220-y

Forsythe N, Fowler HJ, Li X-F, Blenkinsop S, Pritchard D (2017) Karakoram temperature and glacial melt driven by regional atmospheric circulation variability. Nat Clim Chang 7:664

Fu Y et al (2018) Precipitation characteristics over the steep slope of the Himalayas in rainy season observed by TRMM PR and VIRS. Clim Dyn 51:1971–1989
Gang C, Yi M, Singer ND, Jian L (2011) Testing the Clausius-Clapeyron constraint on the aerosol-induced changes in mean and extreme precipitation. Geophys Res Lett 38:37–53
Held IM, Soden BJ (2006) Robust responses of the hydrological cycle to global warming. J Clim 19:5686–5699. https://doi.org/10.1007/s11442-013-1021-y
Hoegh-Guldberg O, Jacob D, Taylor M, Bindi M, Brown S, Camilloni I, Diedhiou A, Djalante R, Ebi KL, Engelbrecht F, Guiot J, Hijioka Y, Mehrotra S, Payne A, Seneviratne SI, Thomas A, Warren R, Zhou G (2018) Impacts of 1.5°C Global Warming on Natural and Human Systems. In: Masson-Delmotte V, Zhai P, Pörtner H-O, Roberts D, Skea J, Shukla PR, Pirani A, Moufouma-Okia W, Péan C, Pidcock R, Connors S, Matthews JBR, Chen Y, Zhou X, Gomis MI, Lonnoy E, Maycock T, Tignor M, Waterfield T (eds) Global Warming of 1.5°C. An IPCC Special Report on the impacts of globalwarming of 1.5°C above pre-industrial levels and related global greenhouse gas emission pathways, in the context of strengthening the global response to the threat of climate change, sustainable development, and effortto eradicate poverty In Press
Hong W, Fubao S, Wenbin L (2018) The dependence of daily and hourly precipitation extremes on temperature and atmospheric humidity over China. J Clim 31:8931–8944
Immerzeel WW, Bierkens MFP (2012) Asian water towers: more on monsoons–response. Science 330:585–585
Ji Z, Kang S, Cong Z, Zhang Q, Yao T (2015) Simulation of carbonaceous aerosols over the Third Pole and adjacent regions: distribution, transportation, deposition, and climatic effects. Clim Dyn 45:2831–2846. https://doi.org/10.1007/s00382-015-2509-1
Jones H, R. SW, Sharma A (2010) Observed relationships between extreme sub-daily precipitation, surface temperature, and relative humidity. Geophys Res Lett 37:L22805
Kang S, Xu Y, You Q, Flügel W-A, Pepin N, Yao T (2010) Review of climate and cryospheric change in the Tibetan plateau. Environ Res Lett 5:015101. https://doi.org/10.1088/1748-9326/5/1/015101
Kharin VV, Zwiers FW, Zhang X, Wehner M (2013) Changes in temperature and precipitation extremes in the CMIP5 ensemble. Clim Chang 119:345–357
Knapp AK et al (2008) Consequences of more extreme precipitation regimes for terrestrial ecosystems. BioScience 58:811–821
Koenker R (2009) Quantreg: quantile regression. https://www.cranr-projectorg/package=quantreg
Lenderink G, Attema J (2015) A simple scaling approach to produce climate scenarios of local precipitation extremes for the Netherlands. Environ Res Lett 10:085001
Lenderink G, Erik M (2010) Linking increases in hourly precipitation extremes to atmospheric temperature and moisture changes. Environ Res Lett 5:025208. https://doi.org/10.1088/1748-9326/5/2/025208
Lenderink G, MH Y, C. LT, J. vOG (2011) Scaling and trends of hourly precipitation extremes in two different climate zones – Hong Kong and the Netherlands. Hydrol Earth Syst Sci 15:3033–3041
Lochbihler K, Lenderink G, Siebesma AP (2017) The spatial extent of rainfall events and its relation to precipitation scaling. Geophys Res Lett 44:8629–8636. https://doi.org/10.1002/2017gl074857
Loriaux JM, Lenderink G, De Roode SR, Siebesma AP (2013) Understanding convective extreme precipitation scaling using observations and an entraining plume model. Journals of the Atmospheric Sciences 70:3641–3655
Min SK, Zhang X, Zwiers FW, Hegerl GC (2011) Human contribution to more-intense precipitation extremes. Nature 470:378–381
Mishra V, Wallace JM, Lettenmaier DPJGRL (2012) Relationship between hourly extreme precipitation and local air temperature in the United States. Geophys Res Lett 39:L16403
Molnar P, Fatichi S, Gaál L, Szolgay J, Burlando P (2015) Storm type effects on super Clausius–Clapeyron scaling of intense rainstorm properties with air temperature. Hydrol Earth Syst Sci 19:1753–1766. https://doi.org/10.5194/hess-19-1753-2015
O'Gorman PA, Muller CJ (2010) How closely do changes in surface and column water vapor follow Clausius–Clapeyron scaling in climate change simulations? Environ Res Lett 5:025207
O'Gorman PA, Schneider T (2009) The physical basis for increases in precipitation extremes in simulations of 21st-century climate change. Proc Natl Acad Sci U S A 106:14773–14777
Pall P, Allen MR, Stone DA (2007) Testing the Clausius-Clapeyron constraint on changes in extreme precipitation under CO_2 warming. Clim Dyn 28:351–363
Panthou G, Mailhot A, Laurence E, Talbot G (2014) Relationship between surface temperature and extreme rainfalls: a multi-time-scale and event-based analysis. J Hydrometeorol 15:1999–2011
Park IH, Min S-K (2017) Role of convective precipitation in the relationship between sub-daily extreme precipitation and temperature. J Clim 30:9527–9537
Qiu, Jane (2007) Environment: riding on the roof of the world. Nature 449:398–402

Roderick ML, Sun F, Lim WH, Farquhar GD (2014) A general framework for understanding the response of the water cycle to global warming over land and ocean. Hydrol Earth Syst Sci 18:1575–1589. https://doi.org/10.5194/hess-18-1575-2014

Schroeer K, Kirchengast G (2017) Sensitivity of extreme precipitation to temperature: the variability of scaling factors from a regional to local perspective. Clim Dyn 50:3981–3994. https://doi.org/10.1007/s11859-006-0311-y

Shaw SB, Royem AA, Riha SJ (2011) The relationship between extreme hourly precipitation and surface temperature in different hydroclimatic regions of the United States. J Hydrometeorol 12:319–325. https://doi.org/10.1175/2011jhm1364.1

Stocker TF et al. (2013) Climate change 2013. The Physical Science Basis. Working Group I Contribution to the Fifth Assessment Report of the Intergovernmental Panel on Climate Change-Abstract for decision-makers

Tan, H.Y M (2016) Monotonic quantile regression with Bernstein polynomials for stochastic. Simulation Technometrics:180–190

Trenberth KE (1999) Conceptual framework for changes of extremes of the hydrological cycle with climate change. Clim Chang 42:327–339

Trenberth KE, Shea DJ (2005) Relationships between precipitation and surface temperature. Geophys Res Lett 32:L14703. https://doi.org/10.1029/2005gl022760

Trenberth KE, Dai A, Rasmussen RM, Parsons DB (2003) The changing character of precipitation. Bull Am Meteorol Soc 84:1205–1218

Vautard R et al (2007) Summertime European heat and drought waves induced by wintertime Mediterranean rainfall deficit. Geophys Res Lett 34:L07711. https://doi.org/10.1029/2006gl028001

Wang S, Zhang M, Wang B, Sun M, Li X (2013) Recent changes in daily extremes of temperature and precipitation over the western Tibetan Plateau, 1973–2011. Quat Int 313-314:110–117. https://doi.org/10.1016/j.quaint.2013.03.037

Wang R et al (2019) Relationship between extreme precipitation and temperature in two different regions: the Tibetan Plateau and Middle-East China. Journal of Meteorological Research 33:870–884. https://doi.org/10.1007/s13351-019-8181-3

Wasko C, Nathan R (2019) The local dependency of precipitation on historical changes in temperature. Clim Chang 156:105–120. https://doi.org/10.1007/s00382-006-0180-2

Wasko C, Sharma A (2014) Quantile regression for investigating scaling of extreme precipitation with temperature. Water Resour Res 50:3608–3614. https://doi.org/10.1002/2013wr015194

Wasko C, Lu WT, Mehrotra R (2018) Relationship of extreme precipitation, dry-bulb temperature, and dew point temperature across Australia. Environ Res Lett 13:074031. https://doi.org/10.1088/1748-9326/aad135

Westra S, Alexander LV, Zwiers FW (2013) Global increasing trends in annual maximum daily precipitation. J Clim 26:3904–3918

Willett KM, Jones PD, Thorne PW, Gillett NP (2010) A comparison of large scale changes in surface humidity over land in observations and CMIP3 general circulation models. Environ Res Lett 5:025210

Xiong J, Ye C, Cheng W, Guo L, Zhou C, Zhang X (2019) The spatiotemporal distribution of flash floods and analysis of partition driving forces in Yunnan Province. Sustainability 11:2926. https://doi.org/10.1002/joc.4239

Xu W, Li Q, Wang XL, Yang S, Cao L, Feng Y (2013) Homogenization of Chinese daily surface air temperatures and analysis of trends in the extreme temperature indices. Journal of Geophysical Research: Atmospheres 118:9708–9720. https://doi.org/10.1002/jgrd.50791

Zhang W, Villarini G (2017) Heavy precipitation is highly sensitive to the magnitude of future warming. Clim Chang 145:249–257

Zhang X, Zwiers FW, Li G, Wan H, Cannon AJ (2017) Complexity in estimating past and future extreme short-duration rainfall. Nat Geosci 10:255–259. https://doi.org/10.1038/ngeo2911

Zhang W, Villarini G, Wehner M (2019) Contrasting the responses of extreme precipitation to changes in surface air and dew point temperatures. Clim Chang 154:257–271. https://doi.org/10.1007/s10584-019-02415-8

Zhao T, Dai A, Wang J (2012) Trends in tropospheric humidity from 1970 to 2008 over China from a homogenized radiosonde dataset. J Clim 25:4549–4567. https://doi.org/10.1175/jcli-d-11-00557.1

Zhou B, Wen QH, Xu Y, Song L, Zhang X (2014) Projected changes in temperature and precipitation extremes in China by the CMIP5 multimodel ensembles. J Clim 27:6591–6611

Zhu Y, Liu H, Ding Y, Zhang F, Lie W (2015) Interdecadal variation of spring snow depth over the Tibetan Plateau and its influence on summer rainfall over East China in the recent 30 years. Int J Climatol 35:3654–3660

Affiliations

Zhiwei Yong [1] · Junnan Xiong [1,2] · Zegen Wang [1] · Weiming Cheng [2] · Jiawei Yang [1] · Quan Pang [1]

✉ Junnan Xiong
neu_xjn@163.com

Zhiwei Yong
yongzhiwei100@163.com

Zegen Wang
zegen01@126.com

Weiming Cheng
chengwm@lreis.ac.cn

Jiawei Yang
yangjw0123@126.com

Quan Pang
pangquan0715@163.com

[1] School of Geoscience and Technology, Southwest Petroleum University, 8, Xindu Road, Xindu District, Chengdu 610500, China

[2] State Key Laboratory of Resources and Environmental Information System, Institute of Geographic Science and Natural Resources Research, Chinese Academy of Sciences, Beijing 100101, People's Republic of China